Construction Materials
Volume 168 Issue CM1

Wood coating failures against natural and accelerated climates
Gupta, Jelle, Hovde and Gao

ice | proceedings

Proceedings of the Institution of Civil Engineers
Construction Materials 168 February 2015 Issue CM1
Pages 3–15 http://dx.doi.org/10.1680/coma.13.00022
Paper 1300022
Received 30/08/2013 Accepted 09/01/2013
Published online 14/08/2014
Keywords: codes of practice & standards/service life/timber structures

ice Institution of Civil Engineers publishing

Wood coating failures against natural and accelerated climates

Barun Shankar Gupta MS, MSc
PhD Research Fellow, Norwegian University of Science and Technology (NTNU), Department of Civil and Transport Engineering, Trondheim, Norway

Bjørn Petter Jelle PhD
Professor, Norwegian University of Science and Technology (NTNU), Department of Civil and Transport Engineering, Trondheim, Norway; SINTEF Building and Infrastructure, Department of Materials and Structures, Trondheim, Norway

Per Jostein Hovde PhD
Professor Emeritus, Norwegian University of Science and Technology (NTNU), Department of Civil and Transport Engineering, Trondheim, Norway

Tao Gao PhD
Research Scientist, Norwegian University of Science and Technology (NTNU), Department of Civil and Transport Engineering, Trondheim, Norway

Monitoring, assessment and prediction of service life of materials are a serious challenge for the building and construction sector. According to ISO 15686 (2008), laboratory testing must be performed alongside field testing to evaluate different degradation outcomes. Coated wooden specimens, used for building façades, were exposed to different ageing conditions in (*a*) a vertical climate simulator, (*b*) a horizontal Atlas solar simulator and (*c*) against natural outdoor exposure conditions. Wood specimens were from Norway spruce grown at two locations in southern Norway. Wooden boards were surface finished by a primer and red acrylate paint. Ageing cycles in the laboratory include exposure to ultraviolet and infrared radiation, water spray, freezing and thawing. Non-destructive surface evaluation techniques were used to monitor and verify the effect of ageing stresses on coatings. Before and after exposure, the coated surfaces were graded visually. Short- and long-term exposures are observed to cause physical degradation such as flaking, cracking and blistering. Blistering on the knots occurs during initial phases of exposure. Different correlations are observed between the CIELab/CIE 1976 coating total colour difference and partial colour difference for artificially aged coated surfaces, naturally aged coated surfaces, and artificially aged uncoated surfaces. Fourier transform infrared spectra suggest possible degradation of wood or coatings during the ageing cycles and a higher content of carbonyl groups in aged acrylate coating. Arrhenius temperature and humidity acceleration factor shows higher rate of deterioration of cellulose, lignin and acrylate in humid conditions.

Notation

a^*	CIE value for redness
b^*	CIE value for yellowness
L^*	CIE value for lightness
ΔC^*_{ab}	CIE a,b chroma difference
ΔE	CIE a,b colour difference
τ	polymer lifetime
$\tau^{(a)}$	athermic stage component
$\tau^{(f)}$	thermofluctuation stage component

1. Introduction

Wood has been used as a building material since ancient times. In northern and central Europe and in many other countries around the world, wood is used as an outdoor cladding (façade) and roofing material. However, wood is a biodegradable material. Moreover, it is chemically heterogeneous and has anisotropic properties. Monitoring of wood degradation in various forms has been of research interest for nearly a century (Kollmann, 1968). Solar radiation, insects, fungi, water and moisture are the main degradation agents for wood. Surface-coated wood provides better resistance against natural degradation agents and longer service life. Contrarily, damage and removal of surface coating exposes the substrate surface that may accelerate wood degradation and further coating delamination. Weathering study procedures are part of the service life prediction of materials as described in the ISO 15686 standards (ISO 15686-1; ISO 15686-2; ISO 15686-8 (ISO, 2000, 2001, 2008a)). Systematic evaluation of properties is required to predict service life of a component.

The longer is the renewal period for the coated façade, the lower is the maintenance cycle and the greater is the service life (NS EN 1995-1-1, CEN, 2004; Steer, 2001). Colour fading is undesirable, as material colour is the aesthetic property that is often given preference by architects and users over other properties to add value to the component. Assessment of the Commission Internationale d'Eclairage (CIE) colour parameters L^*, a^* and b^* are recommended procedures to quantify colour changes. Previously, it was observed that the major

changes in colour were obtained from L^* values (Bagheri *et al.*, 2005). A statistically significant relationship could not be obtained between surface finish and the colour; however, darker colours were obtained at values over 3·3 of colour difference (ΔE) (Bagheri *et al.*, 2005). In another study, it was found that the discoloration due to staining agents occurs at mean ΔE values of 3·7 or above (Guler *et al.*, 2005). Surface morphology, polishing techniques and surface ingredients affect the ΔE values (Sanmartin *et al.*, 2011). The reported threshold values of ΔE perceptible by human eye are in the following classes: range of 2–3 is perceptible, values from 3 to 8 are moderately perceptible, and values above 8 are markedly perceptible (Sarac *et al.*, 2006). Furthermore, in another study, it was observed that the surface roughness has a distinctive effect on the colour properties (da Costa *et al.*, 2007, 2010).

Degradation of methyl-methacrylate coatings occurs by short-chain fragmentation that increases due to intramolecular transfer processes. These processes introduce terminal carbon–carbon unsaturation that can be observed as changes in infrared (IR) absorption in the Fourier transform infrared (FTIR) spectroscopic fingerprint region (Allen *et al.*, 1996). On the other hand, interaction between ultraviolet (UV) radiation and the titanium dioxide (TiO_2) in the coating formulation produces free radicals that degrade the binder and cause discoloration (Allen *et al.*, 2002, 2004). The radiation-induced ageing breaks down the poly-methyl-methacrylate into smaller fragments of a size comparable to the monomer methyl-methacrylate (Tsoi *et al.*, 2004). Bulcke *et al.* (2008) found that the change in the ΔE for exterior wood coating systems is larger for semi-transparent systems than for opaque systems. Additionally, the researchers observed that a solvent-borne semi-transparent system performed better than water-borne systems (Bulcke *et al.*, 2008).

Wood degradation is a complex process (Brischke *et al.*, 2008; Faix, 1988; Felix and Morlier, 1992; Frandsen *et al.*, 2007; Greubel, 1987; Grull and Anderl, 2004; Gupta *et al.*, 2010, 2011; Skaar, 1984). Wood anatomy, microstructure, surface roughness, surface chemistry and tree growth conditions affect the natural outdoor weathering phenomena (Kollmann, 1968; Lewin and Goldstein, 1991). Popescu *et al.* (2006) performed FTIR studies on 150–270-year-old lime wood and observed that the hydrogen bond energy (E_H) increases with the age of wood, indicating removal of molecules forming weaker bonds, providing continuity to the existing strongly bonded interactions. It is a challenging task to combine wood properties with coating properties to describe the degradation process of a coated surface in natural outdoor ageing conditions. Artificial ageing is a controlled process that provides valuable information in a manipulated condition. Ageing methods can be accelerated in various ways (Mohammadian *et al.*, 2010). In an artificial ageing process, the cycle of exposure strains provide environmental stresses within a shorter period of time, thereby, making prediction of service life faster than by the normal natural outdoor test (ISO 2810 and ISO 16053 (ISO, 2004, 2010)).

In our work reported herein, façade materials were exposed to the radiation vertically, tilted and horizontally. The research plan of this study was to monitor and evaluate the damages that occurred to the coated wooden façade surfaces by

(*a*) artificial ageing in a vertical climate simulator, with specimen mounted vertically
(*b*) artificial ageing in an Atlas solar simulator, with specimen mounted horizontally
(*c*) natural outdoor ageing at inclinations of 90° and 45°.

The research objectives were to

(*a*) quantify the damage levels of coatings for all types of exposures
(*b*) evaluate changes in coating properties during exposures
(*c*) assess the effect of wood growth conditions on surface coating degradation.

2. Experimental

2.1 Materials

Coated wood specimens of spruce (*Picea abies* [L] Karst.) were used as supplied by the Norwegian University of Life Sciences (UMB) and Jotun AS, Norway. Geographically, the wood specimens were obtained from timber cut at two nutrient-rich sites at Toten (60°37′N, 10°53′E) and two nutrient-poor sites at Larvik (59°4′N, 10°0′E) in south-eastern Norway. Trees from the poor sites grow slowly and have dominant heights of <14 m whereas trees from the fertile sites have dominant heights of >20 m. Trees at the nutrient-rich sites had large annual ring widths and the trees from the nutrient-poor sites had small annual ring widths. The sawn logs were further classified into small (breast height diameter = 27–30 cm) and large (32–35 cm). The sawing patterns were followed to obtain boards as per previous study (Sivertsen, 2010). The wooden planks (19 cm × 98 cm × 80 cm) were kiln dried, cut into smaller sized panels, planed, conditioned and spray coated with a primer and a commercially available acrylate red coating (Jotun Industri Optimal, viscosity DIN 4 cup 70–90 s, pH 8·0–8·5). All specimens were edge sealed with a yellow-coloured, moisture-impermeable paint to prevent edge cracking. The rear sides of the panels were left uncoated. Exposures were performed at the tangential surfaces and radial surfaces of the wood.

2.2 Vertical climate simulator exposure

Coated specimens of dimensions ~2 cm × 10 cm × 20 cm were exposed and monitored in a vertical climate simulator for 19 months until all specimens developed crack failure. The

vertical simulator works by stepwise rotating a set of specimens to the following exposure conditions: (*a*) UV and IR radiation heat chamber, (*b*) cold water (10℃, 100% relative humidity (RH)) spray chamber at an effective rate of 15 $dm^3/(m^2\ h)$, (*c*) freezing chamber (−20℃) and finally (*d*) the ambient laboratory room conditions. The specimens were exposed to each of the four climate strains for a total length of 365 days × 6 times/day × 1 h/time = 2190 h per year. The details are described in a published test method (Nordtest Method NT Build 495, 2000). At each climate strain condition the specimens were exposed for 1 h duration. The black panel temperature in the UV and IR climate chamber was about 63℃. Visual inspection was performed along with the inspection by colour meter during the ageing period.

2.3 Atlas solar simulator exposure

For ageing testing in the Atlas SC600 MHG solar simulator (Vötsch Industrietechnik GmbH, Germany), uncoated material (six specimens) was used for control specimens, alongside the coated materials (six specimens). Coated and uncoated materials of dimensions ~2 cm × 10 cm × 10 cm were exposed according to a cyclic procedure for altogether 42 days comprising: (*a*) 5 h solar radiation (Osram Metalogen 2500 W, Germany) and (*b*) 1 h water spray (10℃). During the solar radiation exposure, temperature and RH were held constant at 63℃ and 50% RH. During the water spray period the temperature and RH were held at 10℃ and 100% RH. Deionised water was sprayed from two nozzles at the rate of 0·5 dm^3/min per nozzle. The specimens were placed horizontally and tilted at a small angle to allow the water to flow off the specimen surface.

2.4 Natural outdoor exposure

Coated specimens of dimensions ~2 cm × 10 cm × 20 cm were mounted facing south at an open test site in Trondheim, Norway (63°25′N, 10°26′E). In total 36 coated specimens were mounted at an angle of 45° and 31 coated specimens were mounted at an angle of 90° to the horizontal plane. The specimens were checked periodically (twice per year) for coating failures for 3 years. Meteorological measurement facilities from the Norwegian Meteorological Institute for registration of daily precipitation, wind direction and solar radiation were pre-installed at the test site (Rüther, 2011). However, no meteorological information was used for colour analysis.

2.5 Visual inspection

A slightly modified specification based on two standards (EN 927-3 and EN 927-6 (CEN, 2000, 2006)) was followed to make test reports of specimens exposed to all types of exposure conditions. The mandatory parameters of evaluation were blistering, cracking and flaking of the coating film. Additionally, substrate surface cracking and knot defects were also recorded.

2.6 Colour measurement

A handheld Mercury Datacolor (USA) instrument with standard D65 illuminant was used at ambient temperature (~23℃) and room RH for the measurement of surface colour and calculation of colour differences in CIELab colour coordinates. Before measurement, each specimen was wiped off by a lint-free cotton paper to remove surface moisture and conditioned for 30 min at room temperature. Measurements were recorded at the middle of the exposed surface. Commission Internationale d'Eclairage (CIE) colour parameters of coated surfaces were determined (ISO 11664-4 and CIE S 014-4/E:2007 (ISO, 2008b)). Values of L^*, a^* and b^* were recorded directly from the colorimeter, where L^* value represents the lightness, a^* represents redness and b^* represents the yellowness. The CIE 1976 a,b chroma difference (ΔC^*_{ab}) and the CIE 1976 a,b colour difference (ΔE) between two colour stimuli is calculated relative to a standard white tile as the Euclidean distance between the points representing them in the space (ISO 11664-4 and CIE S 014-4/E:2007 (ISO, 2008b)).

$$1.\quad \Delta E = \sqrt{(\Delta L^*)^2 + (\Delta a^*)^2 + (\Delta b^*)^2}$$

$$2.\quad \Delta C^*_{ab} = \sqrt{(\Delta a^*)^2 + (\Delta b^*)^2}$$

2.7 FTIR spectroscopy

Three replicates of attenuated total reflectance (ATR) Fourier transform infrared (FTIR) spectra were obtained on a Nicolet 8700 FTIR Spectrometer (Thermo Scientific). Small flakes of surface coatings were peeled off by a pair of clean tweezers from the red-coated wood specimen surfaces. Two series of spectra were recorded: (*a*) the air–coating interface that had suffered climate stresses from outside and (*b*) the wood–coating interface that was adhered inward to the wood. The mid-IR region of 4000–400 cm^{-1} was selected.

2.8 Statistical evaluation

A linear regression analysis of data points from the colorimeter readings was performed. Coefficient of determination (R^2) is provided to check the variability explained by the linear regression model (α = 0·05).

3. Results and discussion

3.1 Visual inspection

Visual gradings of the specimen surfaces were assessed by the following properties – flaking, cracking, mould growth, loose knots, chalking, blistering and appearance. Each panel was examined, in between exposure periods, after absorbing the surface moisture by clean cotton soft wipes.

3.1.1 Vertical climate simulator exposure

The aged specimens showed occurrence of surface cracks and edge cracks/end splits after a few months of exposure in the vertical climate simulator. Figure 1 shows that after some exposure time to each climate strain, 100% of the exposed specimens had noticeable, deep, through-and-through cracks that initiated at the edges. Periodic swelling and shrinkage of the wood at short, repeated intervals due to water sorption and heat conditioning could be the causes. The heat generated in the UV and IR chamber gave a surface temperature of ~63℃ (black panel temperature) and probably aids in faster degradation, along with the energy-carrying photons. Ice is not considered to be a degradation agent for wood. However, there is volume expansion when water freezes to ice that could result in micro-cracks and tearing off wood fibres at the meso-scale. Specimens with knots recorded loose knot behaviour. Moreover, cupping and warping defects were also present in specimens after 1 year of exposure in the vertical climate simulator.

3.1.2 Atlas solar simulator exposure

Figure 2 shows that the specimens exposed in the Atlas solar simulator showed damage behaviour similar to the vertical climate simulator specimens. Surface checks and falling off of dead knots from the coated and uncoated surfaces were observed. Altering exposure conditions causes surface elongation and surface micro-cracks in the specimens. More than 40% of the coated specimens developed flaking after 6 weeks of exposure. Coating cracks were observed in 25% of the specimens after 6 weeks of exposure. After the total exposure period, all uncoated specimens showed warping, which was absent in the coated specimens. Also, the number of edge cracks and crack lengths was much higher for uncoated specimens. Resin streaks and resin pitches were found on the uncoated specimens after exposure. The late wood parts were darker than early wood parts. Moreover, the aged wood specimens appeared greyish and shiny compared to the fresh wood surfaces.

3.1.3 Natural outdoor exposure

Figure 3 shows the damage that occurred in specimens mounted outdoors in wooden frames at an angle of 45° and facing south. After the first 6 months of exposure, more than 60% of the specimens showed surface/edge cracking and blistering from painted knots. Flaking and blistering of coatings from other parts of the surfaces were observed in less than 10% of the specimens. Flaking continued to increase throughout the exposure period and was found in more than 50% of the specimens after 3 years of exposure, while blistering was negligible. Nearly 70% of the specimens showed surface cracks and checks through the coating after 3 years of exposure.

Figure 4 shows the damages that occurred in specimens that were mounted outdoors vertically (90°) for natural climate exposure. Changes in the types and extent of damage that occurred were observed due to seasonal variation of weather, which exposed the wood specimens to various amounts of solar radiation and humidity, at different periods of time. After the first 6 months of exposure, more than 50% of the specimens showed blistering from painted knots and less than 10% of the specimens

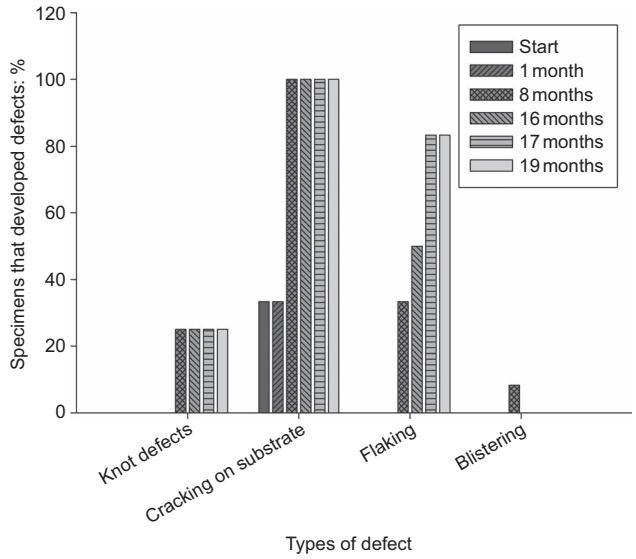

Figure 1. Defects in coated specimens from exposure in the vertical climate simulator

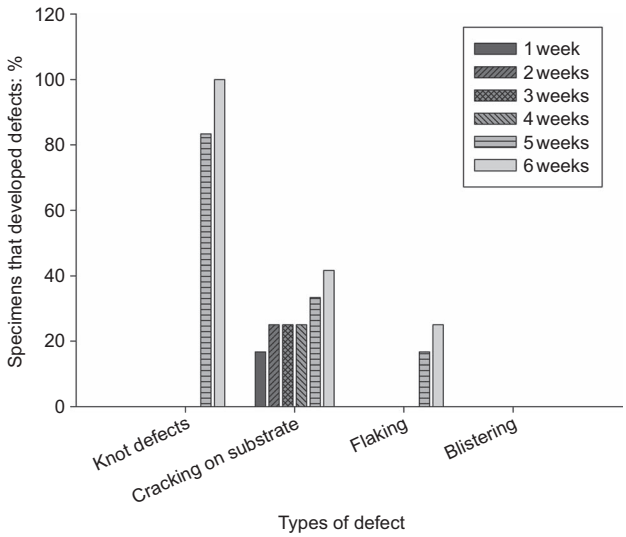

Figure 2. Defects in coated specimens from exposure in the Atlas solar simulator

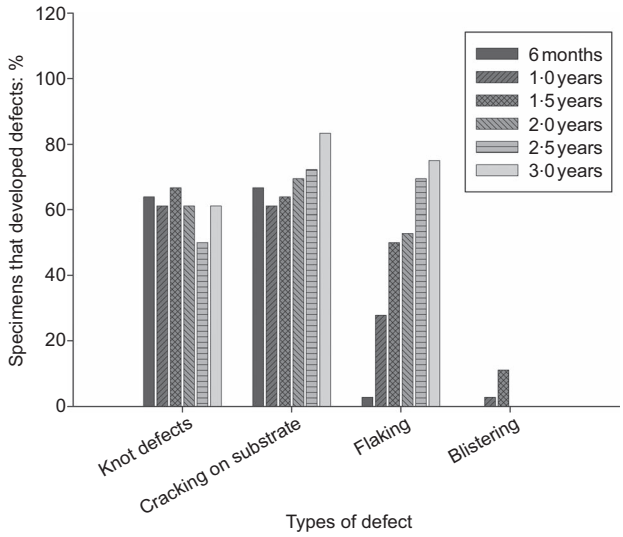

Figure 3. Defects in coated specimens at 45° inclination in the natural outdoor climate exposure

showed surface cracking. Flaking and blistering of coatings from other parts of the surfaces were not found. Flaking and surface/edge cracking continued to increase and were found in more than 50% of the specimens after 3 years of exposure. During ageing, water might have penetrated through the failed coating and swelled the wood substrate underneath. The swollen woods have possibly reduced the gaps surrounding the knots, resulting in the decline in knot failure at later stages. No mould growth on the coating surfaces was observed during the study.

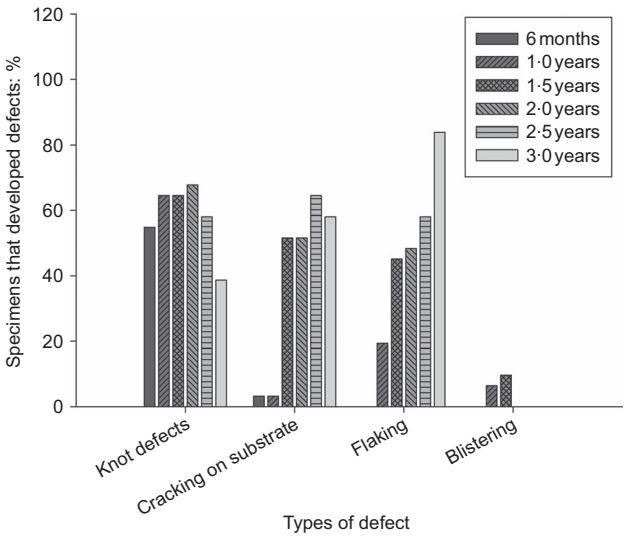

Figure 4. Defects in coated specimens at 90° inclination in the natural outdoor climate exposure

It may seem that failure as surface cracks occurs at a faster rate in boards mounted at 45° and facing south than that of the vertically mounted boards.

It is generally believed that radial sawn boards perform better than boards produced using other types of sawing patterns. However, no particular trend was observed between the sawing pattern and the coating failure occurrences during these short periods of exposure. Probably, small specimen dimensions and improper sampling were the reason for this observation. For evaluation of long-term failure, further research is needed.

3.2 Colour measurements

The CIELab system has practical application by explaining every colour by a single point in the Cartesian tri-chromatic space. $L^*a^*b^*$ are the colour coordinates. The lightness of the specimen (L^*) ranges between 0 (black) and 100 (white). The other colour coordinates, a, range from −150 to +150. The colour coordinate (+) a^* signifies a colour shift towards red and (−) a^* towards green. The colour coordinate (+) b^* signifies colour shift towards yellow and (−) b^* signifies colour shift towards blue. The values of each colour coordinate are shown in Table 1. Moreover, from Table 1 it is possible to conclude that among the artificial exposures performed, it was the exposure in the Atlas solar simulator that provided maximum damage as per ΔE value. Additionally, the total colour changes $\Delta E_{(\text{final} - \text{initial})}$ for the uncoated surfaces are 27 ± 6, which comes below visible perception of the human eye, as defined in previous literature (Sarac *et al.*, 2006). So, among all the exposures performed in this study, it is the colour changes of uncoated surfaces that became noticeable by human eye; the colour changes of coated surfaces were beyond recognition by the human eye.

3.2.1 Vertical climate simulator exposure

Table 1 shows that there is a decreasing trend in L^* values for coated surfaces with increasing exposure duration. Lightness, L^*, is most affected by changes in the roughness of the surface (Sanmartin *et al.*, 2011). So, it may be concluded that the coating colour lightness changes due to roughness imparted by degradation agents like electromagnetic, thermal, chemical and/or mechanical agents from both types of artificial exposure climate conditions. The a^* and C^* values show an increasing trend with higher exposure duration. Figure 5 shows that in the vertical climate simulator the coating colour intensity shifts towards higher chroma with ageing. Regression analysis shows a strong positive linear trend with 89% of the variation being explained by the linear model. Environmentally, the difference between the horizontal and vertical types of exposure is in the

Exposure types		L^*	a^*	b^*	C^*_{ab}	Total colour change, $\Delta E_{(\text{final} - \text{initial})}$
Vertical climate simulator/coated[a]	Start	36·7 ± 0·3	25·4 ± 0·2	16·8 ± 0·2	30·5 ± 0·3	4 ± 1
	7 months	35·6 ± 0·6	26·4 ± 0·6	18·5 ± 0·7	32·2 ± 0.9	
	16 months	35·6 ± 0·9	27·3 ± 0·7	19·9 ± 0·8	34 ± 1	
	17 months	35 ± 1	27·0 ± 0·6	19·3 ± 0·8	33 ± 1	
	18 months	35·2 ± 0·7	27·1 ± 0·8	19 ± 1	33 ± 1	
	19 months	35·0 ± 0·9	27 ± 1	20 ± 1	33 ± 2	
Atlas solar simulator/horizontal/coated[a]	Start	36·6 ± 0·1	25·5 ± 0·2	17·2 ± 0·2	30·7 ± 0·3	1·4 ± 0·7
	7 d	36·0 ± 0·4	25·4 ± 0·4	17·0 ± 0·4	30·5 ± 0·6	
	14 d	35·1 ± 0·4	26·5 ± 0·5	18·6 ± 0·6	32·4 ± 0·7	
	21 d	34·9 ± 0·8	26·5 ± 0·5	18·3 ± 0·7	32·2 ± 0·7	
	28 d	36 ± 1	25·7 ± 0·5	17·0 ± 0·8	30·8 ± 0·9	
	35 d	37 ± 1	25·5 ± 0·5	16·9 ± 0·7	30·5 ± 0·8	
Atlas solar simulator/horizontal/uncoated[b]	Start	81 ± 2	3·5 ± 0·7	20 ± 1	20 ± 1	27 ± 6
	7 d	54 ± 5	8 ± 3	22 ± 5	24 ± 5	
	14 d	54 ± 7	7 ± 2	19 ± 4	20 ± 4	
	21 d	55 ± 5	6 ± 2	16 ± 4	17 ± 4	
	28 d	54 ± 6	6 ± 3	15 ± 5	16 ± 6	
	35 d	54 ± 6	5 ± 3	15 ± 4	16 ± 4	
Natural outdoor exposure/90°/coated[c]	Start	36·9 ± 0·2	25·7 ± 0·1	17·1 ± 0·1	30·8 ± 0·2	1·6 ± 0·1
	27 months	36·8 ± 0·2	25·6 ± 0·2	17·4 ± 0·3	31·0 ± 0·2	
	34 months	36·0 ± 0·2	25·0 ± 0·1	16·1 ± 0·2	29·7 ± 0·1	
Natural outdoor exposure/45°/coated[d]	Start	36·9 ± 0·2	25·6 ± 0·2	17·1 ± 0·2	30·8 ± 0·2	2.0 ± 0.3
	27 months	37·0 ± 0·2	25·5 ± 0·3	17·8 ± 0·2	31·1 ± 0·3	
	34 months	35·8 ± 0·3	24·7 ± 0·2	15·8 ± 0·2	29·4 ± 0·3	
White tile (reference)		95·83	−0·14	2·38	–	
Black trap (reference)		0·02	0·02	0·02	–	

[a]Mean of 12 measurements ± uncertainty. The uncertainty is calculated as three times the standard deviation of the mean, i.e. a confidence interval of 99·73 %
[b]Mean of six measurements ± uncertainty
[c]Mean of 31 measurements ± uncertainty
[d]Mean of 36 measurements ± uncertainty

Table 1. CIELab colour coordinates for coated and uncoated surfaces of wood specimens

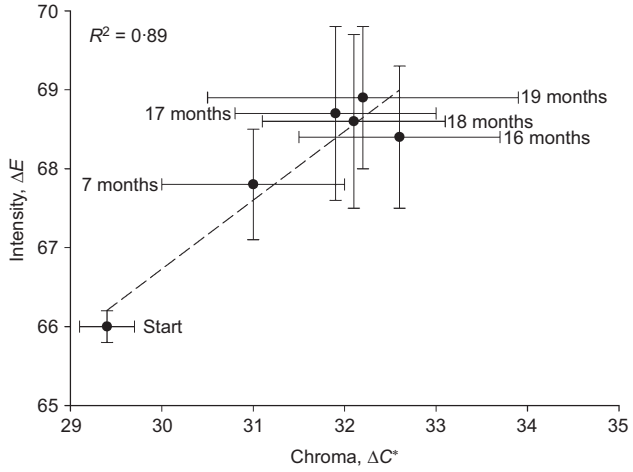

Figure 5. *ΔE–ΔC** curve of red-coated specimens during artificial ageing exposure in the vertical climate simulator

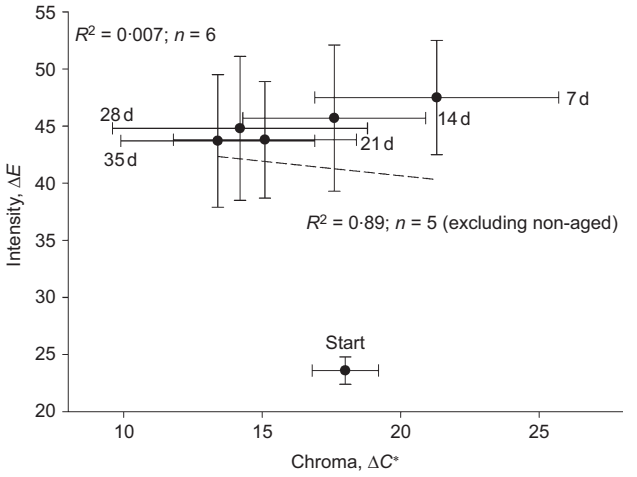

Figure 6. *ΔE–ΔC** graph of uncoated specimens during artificial ageing exposure in the Atlas solar simulator

experimental design; for example, in the vertical climate simulator there is a freezing period which is absent in the horizontal exposure programme.

3.2.2 Atlas solar simulator exposure

The value of the parameter L^*, lightness, varied from 37 to 35 for coated surfaces during the exposure as seen from Table 1. Contrarily, the uncoated surfaces showed initial value of $L^* = 81$, which is near to the $L^* = 95$ of white tile used as a reference. Upon exposure the L^* value of uncoated surface decreased from a mean value of 81 to 54. Similarly, the value of the chromatic parameter a^* varied from 25 to 27 for coated surfaces, while for the uncoated surfaces the range was 4–8. The other chromatic parameter b^* varied between 17 and 19 for coated surfaces and between 15 and 22 for uncoated surfaces. On the other hand, the lowest chroma values (C^*) were obtained for uncoated surfaces. The L^*, a^* and C^*_{ab} values showed a decreasing trend for the uncoated surfaces with higher exposure duration. Figure 6 shows the progress of ageing of uncoated specimens in the Atlas solar simulator. At the beginning, the variation in ΔE and ΔC^*_{ab} have the lowest values. There is an increase in both values immediately after 1 week of exposure. Regression analysis shows that the only few percentage points of variation in intensity is explained by the chroma, indicating a linear regression model cannot be used. These phenomena can be explained from physical observations. The greyness of the surfaces increases until the end of the exposure period. The initial jump in values would have possibly resulted from the shiny woolliness of degraded wood fibres.

Figure 7 shows the ΔE–ΔC^*_{ab} relationship of coated surfaces that have been exposed to cyclic radiation and water spray exposure in the Atlas solar simulator. There is an increase in intensity along with the increase in chroma. Regression analysis fitted a model with $R^2 = 0{\cdot}86$. The maximum temperature during exposure was 63°C. A probable cause for this relationship could be the surface roughness and the high concentration of broken polymer chains at the surfaces generated during radiation exposure, which altered the colour configuration of the surfaces. There are high variations in both chroma and intensity for each recorded period, which indicates the presence of various amounts of degraded products on the surfaces.

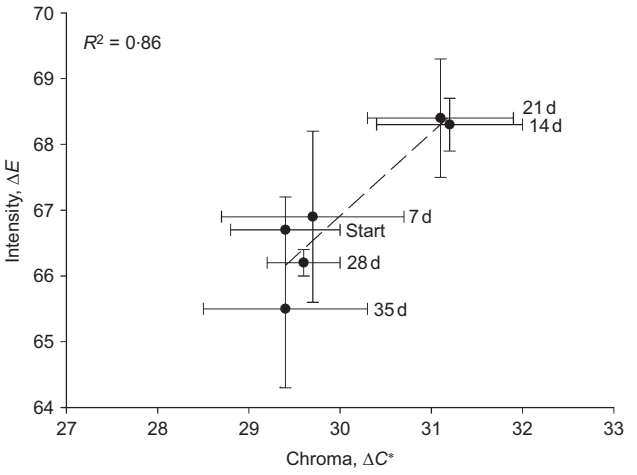

Figure 7. *ΔE–ΔC** graph of red-coated specimens during artificial ageing exposure in the Atlas solar simulator

3.2.3 Natural outdoor exposure

For the natural outdoor exposure case, colour measurements were performed at three different ageing times, namely, at the beginning of the 3 years' exposure (start), before the end (27 months) and at the end of the exposure period (34 months). The value of the parameter L^*, lightness, varied from 36 to 37 for coated surfaces, as in Table 1. Similarly, the value of the chromatic parameter a^* varied from 25 to 26 for coated surfaces. The other chromatic parameter b^* varied within 16–18 for the coated surfaces. There is particularly no difference in the $L^*a^*b^*$ values between surfaces that were exposed at 90° and 45° inclination against natural climate degradation agents. Figures 8 and 9 show that, after ageing by natural outdoor climate exposure, the colour intensity drops with higher chroma. Regression analysis shows that 49% and 88% of the variations can be explained by the linear model. Both types of exposure show a similar pattern in the graphs.

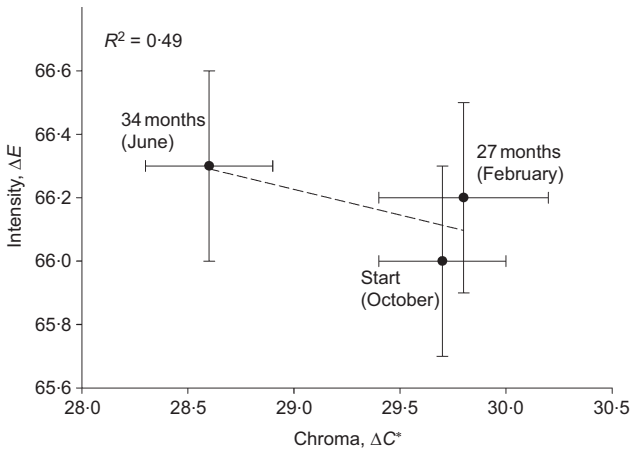

Figure 8. ΔE–ΔC^* graph of red-coated specimens at 90° inclination during natural outdoor climate exposure

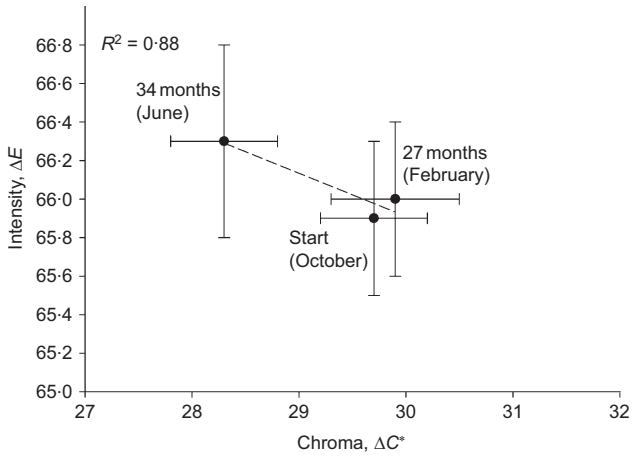

Figure 9. ΔE–ΔC^* graph of red-coated specimens at 45° inclination during natural outdoor climate exposure

3.3 FTIR spectroscopy of coating film–air interface

On wood substrate, a coating film has two interfaces: the air–film interface, which is exposed to the outside climate strains, and the film–wood substrate, which faces towards the wood substrate and is not directly exposed to the climate strains. Figure 10 shows the survey FTIR spectra of the exposed and unexposed coatings. The weak absorption at 3560 cm^{-1} is assigned to hydrogen-bonded oxygen–hydrogen (O–H) stretching vibrations of carboxylic acid. The two peaks at 2960 cm^{-1} and 2872 cm^{-1} are assigned to carbon–hydrogen (C–H) stretching vibrations of the methyl (CH_3) group. The peak at about 2930 cm^{-1} is related to C–H stretching from the methylene CH_2 group, of which the intensity changes provide valuable information with respect to the ageing process, as found by other researchers (Allen *et al.*, 2002). The higher intensity for the O–H stretching band in the exposed coatings may suggest the formation of more hydroxy compounds during the ageing process; in other words, the exposed coating is more hydrophilic than the unexposed coating. Additionally, the (CH_3) and CH_2 peaks are slightly weaker for exposed coating compared to unexposed coating, suggesting removal of alkanes. The peak at 1725 cm^{-1} is assigned to the carbonyl (C=O) stretching vibration of carboxylic acids (Nguyen *et al.*, 2002). The exposed coating shows lower intensity, indicating less amount of carboxyl content. However, the exposed coating shows the appearance of two broad shoulders at 1780 cm^{-1} in the C=O region and 1590–1560 cm^{-1} in the COO^-/N–H region of IR spectra, which are absent in unexposed coating.

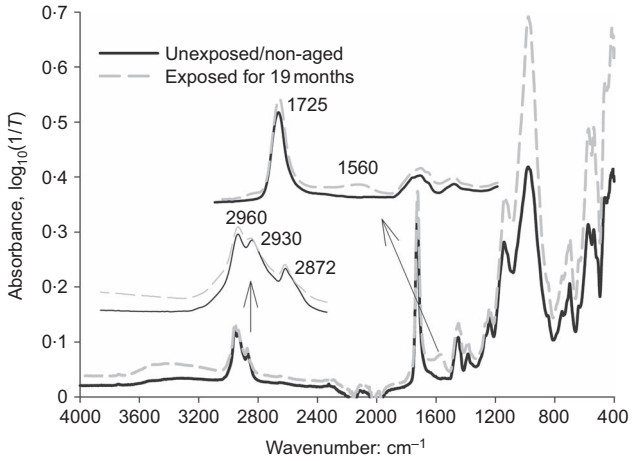

Figure 10. Coating film–air interface: FTIR survey spectra of wood coating exposed to artificial ageing conditions in vertical climate simulator

Figure 11 shows the spectra at lower wavenumbers. Higher intensities for exposed coatings were observed for O–H in-plane bending vibrations at 1420 cm^{-1}, O–H deformation at 950–900 cm^{-1}, CH_2 rocking vibration at 720 cm^{-1} and C–H out-of-plane vibration at 700 cm^{-1}. Overall, it may be said that exposure of the coating to UV radiation and other climate strains increases the hydrophilicity of the compound by increasing the amount of surface hydroxyl group (OH) content.

3.4 FTIR spectroscopy of coating film–wood interface

Figure 12 shows the IR spectra for the coating film facing towards the wood substrate. The broad peak at 3300 cm^{-1} for H-bonded O–H is present for both the unexposed and exposed side of the coating. There is a general dissimilarity in pattern and intensity between the coating film for unexposed and exposed conditions. First, the order of intensities at 2960–2850 cm^{-1} has been changed. Note the changes in the absorption intensities of the IR bands for C–H stretching of (CH_3) groups at 2960 cm^{-1} and 2872 cm^{-1} and the changes in the intensities of the IR bands assigned to C–H stretching vibrations of CH_2 groups at 2930 cm^{-1} and 2856 cm^{-1}. Specifically, there were no visible differences between peaks of the C–H stretching vibrations for (CH_3) and CH_2 groups of the spectra of exposed coating film. Possibly, the heat of exposure has induced structural and conformational changes in the coating at the wood substrate side of the exposed film. Figure 12 shows the spectral pattern to assign C=O stretching vibrations to carboxyl groups. The wood side/unexposed film shows a sharp peak at 1725 cm^{-1} characteristic of the C=O stretching vibrations. For the wood side/exposed film there are two additional peaks at 1640 cm^{-1}, that are characteristic for C=O stretching vibrations of ketones, and another peak at 1540 cm^{-1}, probably due to the amide II of nitrogen–hydrogen (N–H) bending and C–H stretching (Nguyen *et al.*, 2002). The additional peaks for the wood side/exposed film have possibly originated due to the presence of impurities and wood extractives on the coatings. Wood is a highly porous material and the wood extractives may migrate to the surface during thermal ageing and weathering (Gardner *et al.*, 1991; Walinder and Gardner, 1999). Figure 13 shows the spectra for lower wavenumbers of the coating facing towards the wood substrate. Higher intensities for exposed coatings were observed for OH deformation at 950–900 cm^{-1}, CH_2 rocking vibration at 720 cm^{-1} and C–H out-of-plane vibration at 700 cm^{-1}.

Coatings promote accumulation of moisture on the exterior side while providing protection against interior humidity stresses (Grull and Anderl, 2004). Overall, Figures 12 and 13 show that exposure of the coating to UV radiation and other climate strains increases the hydrophilicity of the compound, as indicated by the increased amount of surface OH content.

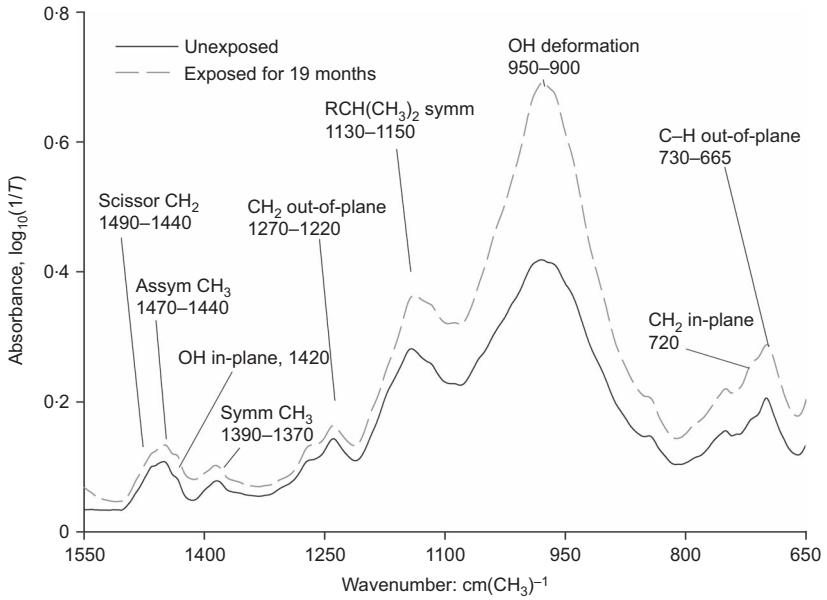

Figure 11. Coating film–air interface: interpretation of FTIR bands for carbon–hydrogen (C–H) groups of red surface coating exposed to artificial ageing conditions in vertical climate simulator (reported also in Figure 10)

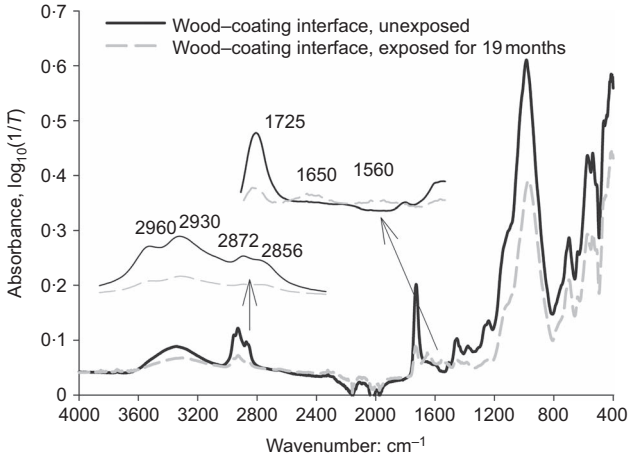

Figure 12. Coating film–wood interface: FTIR survey spectra of the coating film measured on the paint faced inward towards the wood substrate, exposed in vertical climate simulator

3.5 Evaluation of coating failure possibilities

From scanning electron microscope (SEM) image study it was evident that there are formations of macro-cracks, micro-cracks, submicro-cracks and micro-blisters at the failure surfaces of the coating. The aged coating surface showed swelling and small pores.

Photons of lower wavelengths carry more energy than the photons of higher wavelengths. Coating failure depends on the amount of radiation absorbed by the coating. The change of the FTIR band at 1725 cm^{-1} is related to the oxidation process and the band at 1540 cm^{-1} is related to the chain scission process (Nguyen *et al.*, 2002). The porous oxidation front, that is created on the surface, starts moving inside the coating with continuous exposure, depending on the solubility of oxygen in the coating, rate of chemical reactions and the rate of diffusion of the oxygen into the coating (Kiil, 2012). After a critical fraction of polymer chains is broken due to photoinitiated chain scission, the ablation front starts moving inside with loss of coating mass (Kiil, 2012). At the inner side, there is a stability of the oxidation zone; accordingly no damages occur even though there is penetration of radiation. Consequently, the coating film–wood interface shows no increase in the band at 1725 cm^{-1} assigned for oxidation. The brittleness temperature of poly-methyl-methacrylate (PMMA) is assumed to be 244–252 K (Tsoi *et al.*, 2004). The lifetime of a polymer (τ) (Tsoi *et al.*, 2004) is given by

$$\tau = \tau^{(f)} + \tau^{(a)} \quad (3)$$

where, $\tau^{(f)}$ is the component for the thermofluctuation stage and $\tau^{(a)}$ is the component for the athermic stage. The formation of defects takes place in the thermofluctuation mode and development of

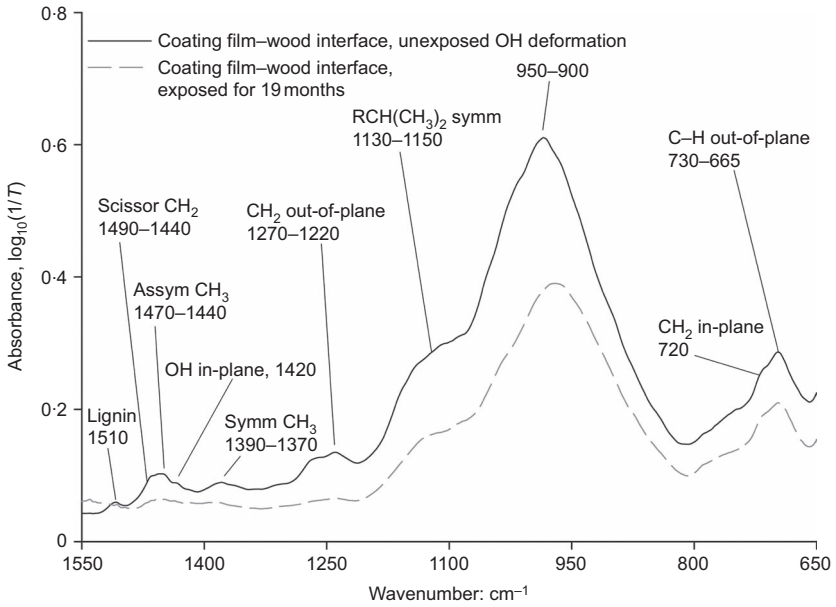

Figure 13. Coating film–wood interface: interpretation of the FTIR spectra of the carbon–hydrogen (C–H) groups of red coating measured on the paint faced inward towards the wood substrate, exposed in vertical climate simulator (reported also in Figure 12)

defects increases at the athermic stage. Moreover, the photodegradation of the coating materials should be faster if they are used above the glass transition temperature. Lifetime decreases with increased stress. Temperature and humidity are both added stresses. Henceforth, the likelihood of coating failure in the vertical climate simulator is higher because this simulator varies the temperature from ice-frost condition to 63℃ (336 K). For more general information and details about accelerated climate ageing in the laboratory it is referred to the study by Jelle (2012) and Jelle *et al.* (2012).

The micro-heterogeneous structures of PMMA could be the reason for failure in applied environmental stresses. The fracture in the coating film progresses due to nucleation of defects and rupture of inter- and intramolecular bonds aided by water. The length of the micro-cracks in PMMA at different stress levels can range between 4 μm and 36 μm (Tsoi *et al.*, 2004).

4. Conclusions

In this study, acrylate-coated wood specimens were exposed for degradation studies. Materials that are used for building façades were aged at three different exposing conditions and the following observations were made.

(*a*) Artificial exposure in the vertical climate simulator revealed coating damages and knot failures earlier than by natural exposure. Flaking, blistering and cracking of the coating were the observed failures. Blistering of the coating had probably hastened due to the freezing temperature applied during exposure, as observed in the microscopic study. Coating ΔE increased linearly (R^2 = 0·89) together with the colour chroma during the exposure period.

(*b*) Artificial exposure in the Atlas solar simulator caused coating failure due to the mixed interaction with the long periods of solar radiation exposure and rainfall. The uncoated wood surface showed the maximum value of L^* among all surfaces tested, indicating whiteness. Additionally, the uncoated surface showed the minimum value of chroma among all the surfaces, showing appearance of blackness. Coating ΔE measured for the uncoated surface failed to project any particular trend with the colour chroma (R^2 = 0·007). However, when the values for non-aged specimen were excluded, there was a good linear fit (R^2 = 0·89). Coating ΔE measured for the red-coated surface showed a linear trend (R^2 = 0·86).

(*c*) Flaking and cracking of coating were the most noticeable failures for natural outdoor climate exposure. A faster occurrence of coating flaking and cracking was observed for the specimens mounted at 45° inclination compared to those mounted at 90°. It was observed that there is an increase in the colour intensity along with loss of greyness. Coating ΔE measured for the red-coated surfaces failed to project any particular trend (R^2 = 0·49) for 45° inclination; however, there seemed to be a linear fit (R^2 = 0·88) for specimens mounted at 90°.

(*d*) FTIR spectra for the groups of interest showed an increase in hydrophilicity and an increase in C=O concentration due to the oxidation and possible degradation of wood/coatings.

(*e*) The total ΔE from the CIELab system showed that the artificial climate strains in the vertical climate simulator did more damage to the coating than the artificial climate conditions in the horizontal Atlas solar simulator, possibly because of the freezing conditions in the vertical simulator.

(*f*) Increased humidity and temperature in combination will accelerate the degradation of wood and coating.

Acknowledgements

The authors would like to thank the Research Council of Norway, Viken Skog BA, Treindustrien, the Wood Technology Research Fund at the Norwegian Institute of Wood Technology, Jotun AS and Kebony ASA for their financial support of the research project. Furthermore, the authors would like to thank the research partners of the project, namely, the Norwegian University of Life Sciences (UMB), the Norwegian Forest and Landscape Institute (Skog og Landskap) and the Norwegian Institute of Wood Technology (Treteknisk). Finally, the authors express their appreciation to Ole Aunrønning, NTNU, for the preparation of specimens and contribution to the experimental studies in the laboratory.

REFERENCES

Allen NS, Regan CJ, McIntyre R, Johnson B and Dunk WAE (1996) The photostabilisation of water-borne acrylic coating systems. *Polymer Degradation and Stability* **52(1)**: 67–72.

Allen NS, Edge M, Ortega A *et al.* (2002) Behaviour of nanoparticle (ultrafine) titanium dioxide pigments and stabilisers on the photooxidative stability of water based acrylic and isocyanate based acrylic coatings. *Polymer Degradation and Stability* **78(3)**: 467–478.

Allen NS, Edge M, Ortega A *et al.* (2004) Degradation and stabilisation of polymers and coatings: nano versus pigmentary titania particles. *Polymer Degradation and Stability* **85(3)**: 927–946.

Bagheri R, Burrow MF and Tyas M (2005) Influence of food-simulating solutions and surface finish on susceptibility to staining of aesthetic restorative materials. *Journal of Dentistry* **33(5)**: 389–398.

Brischke C, Rapp AO, Bayerbach R *et al.* (2008) Monitoring the 'material climate' of wood to predict the potential for decay: results from in situ measurements on buildings. *Building and Environment* **43(10)**: 1575–1582.

Bulcke JVD, Acker JV and Stevens M (2008) Experimental and theoretical behavior of exterior wood coatings subjected to

artificial weathering. *Journal of Coating Technology Research* **5(2)**: 221–231.

CEN (European Committee for Standardisation) (2000) EN 927-3: Paints and varnishes. Coating materials and coating systems for exterior wood. Part 3: Natural weathering test. Brussels, European Committee for Standardisation, Brussels, Belgium.

CEN (2004) NS EN 1995-1-1: Eurocode 5: Design of timber structures – Part 1-1: General – common rules and rules for buildings. CEN, Brussels, Belgium.

CEN (2006) EN 927-6: Paints and varnishes. Coating materials and coating systems for exterior use. Part 6: Exposure of wood coatings to artificial weathering using fluorescent UV lamps and water. European Committee for Standardisation, Brussels, Belgium.

da Costa J, Ferracane J, Paravina RD, Mazur RF and Roeder L (2007) The effect of different polishing systems on surface roughness and gloss of various resin composites. *Journal of Esthetic and Restorative Dentistry* **19(4)**: 214–224.

da Costa J, Adams-Belusko A, Riley K and Ferracane JL (2010) The effect of various dentifrices on surface roughness and gloss of resin composites. *Journal of Dentistry* **38(2)**: E123–E128.

Faix O (1988) Practical uses of FTIR spectroscopy in wood science and technology. *Mikrochimica Acta* **1(1–6)**: 21–25.

Felix S and Morlier P (1992) Modeling of stresses and strains in a piece of wood under drying. *Holzforschung* **46(5)**: 369–377.

Frandsen HL, Damkilde L and Svensson S (2007) A revised multi-Fickian moisture transport model to describe non-Fickian effects in wood. *Holzforschung* **61(5)**: 563–572.

Gardner DJ, Generalla NC, Gunnells DW and Wolcott MP (1991) Dynamic wettability of wood. *Langmuir* **7(11)**: 2498–2502.

Greubel D (1987) Calculating the transport of heat and moisture in wall elements of wood based materials. *Holz Als Roh-und Werkstoff* **45(4)**: 145–149.

Grull G and Anderl T (2004) Wood moisture content of coated wood/aluminium windows Part 2: Reactions to interior humidity stress. *Surface Coatings International Part B – Coatings Transactions* **87(3)**: 203–210.

Guler AU, Yilmaz F, Kulunk T, Guler E and Kurt S (2005) Effects of different drinks on stainability of resin composite provisional restorative materials. *Journal of Prosthetic Dentistry* **94(2)**: 118–124.

Gupta BS, Jelle BP, Hovde PJ and Rüther P (2010) FTIR spectroscopy as a tool to predict service life of wooden cladding. *Proceedings of the 18th CIB World Building Congress, Salford, UK*, CIB Publication 363, pp. 345–356.

Gupta BS, Jelle BP, Hovde PJ and Rüther P (2011) Studies of wooden cladding materials degradation by spectroscopy. *Proceedings of the Institution of Civil Engineers – Construction Materials* **164(6)**: 329–340.

ISO (2000) ISO 15686-1: Building and constructed assets – Service life planning. International Organisation for Standardisation, Geneva, Switzerland.

ISO (2001) ISO 15686-2: Buildings and constructed assets – Service life planning – Part 2: Service life prediction procedures. International Organisation for Standardisation, Geneva, Switzerland.

ISO (2004) ISO 2810: Paints and varnishes – Natural weathering of coatings – Exposure and assessment. International Organisation for Standardisation, Geneva, Switzerland.

ISO (2008a) ISO 15686-8: Buildings and constructed assets – Service life planning – Part 8: Reference service life and service-life estimation, 1st edn. International Organisation for Standardisation, Geneva, Switzerland.

ISO (2008b) ISO 11664-4 and CIE S 014-4/E:2007: Colorimetry – Part 4: CIE 1976 L*a*b* colour space, 1st edn. International Organisation for Standardisation, Geneva, Switzerland.

ISO (2010) ISO 16053: Paints and varnishes – Coating materials and coating systems for exterior wood – Natural weathering test, 2nd edn. International Organisation for Standardisation, Geneva, Switzerland.

Jelle BP (2012) Accelerated climate ageing of building materials, components and structures in the laboratory. *Journal of Materials Science* **47**: 6475–6496.

Jelle BP, Nilsen T-N, Hovde PJ and Gustavsen A (2012) Accelerated climate aging of building materials and their characterization by Fourier transform infrared radiation analysis. *Journal of Building Physics* **36**: 99–112.

Kiil S (2012) Model-based analysis of photoinitiated coating degradation under artificial exposure conditions. *Journal of Coating Technology Research* **9(4)**: 375–398.

Kollmann FPZ (1968) *Principles of Wood Science and Technology – I Solid Wood*. Springer, New York, NY, USA.

Lewin M and Goldstein IS (1991) *Wood Structure and Composition*. Marcel Dekker, New York, NY, USA.

Mohammadian SH, Ait-Kadi D and Routhier F (2010) Quantitative accelerated degradation testing: Practical approaches. *Reliability Engineering and System Safety* **95(2)**: 149–159.

Nguyen T, Martin JW, Byrd E and Embree E (2002) Effects of spectral UV on degradation of acrylic-urethane coatings. *Proceedings of the 80th Annual Meeting of the Program of the FSCT*. Federation of Societies for Coatings Technology, New Orleans, LA, USA.

Nordtest Method NT Build 495 (2000) Building materials and components in the vertical position: Exposure to accelerated climatic strains. Espoo, Finland.

Popescu CM, Vasile C, Popescu MC and Singurel G (2006) Degradation of lime wood painting supports II – spectral characterisation. *Cellulose Chemistry and Technology* **40(8)**: 649–658.

Rüther P (2011) *Wood Weathering from a Service Life Perspective*. PhD thesis, The Norwegian University of Science and Technology, Trondheim, Norway.

Sanmartin P, Silva B and Prieto B (2011) Effect of surface finish on roughness, color, and gloss of ornamental granites. *Journal of Materials in Civil Engineering* **23(8)**: 1239–1248.

Sarac D, Sarac YS, Kulunk S, Ural C and Kulunk T (2006) The effect of polishing techniques on the surface roughness and color change of composite resins. *Journal of Prosthetic Dentistry* **96(1)**: 33–40.

Sivertsen MS (2010) *Liquid Water Absorption in Wood Cladding Boards and Log Sections with and without Surface Treatment*. PhD thesis, Department of Ecology and Natural Resource Management, Norwegian University of Life Sciences, Akershus, Norway.

Skaar C (1984) Wood water relationships. In: R.M. Rowell, ed., The Chemistry of Solid Wood, *Advances in Chemistry Series.* American Chemical Society, U.S.A., Washington, DC **(207)**: 127–172.

Steer PJ (2001) EN 1995 Eurocode 5: Design of timber structures. *Proceedings of the Institution of Civil Engineers – Civil Engineering* **144(6)**: 39–43.

Tsoi B, Kartashov EM and Shevelev VV (2004) *The Statistical Nature of Strength and Lifetime in Polymer Films and Fibers*. VSP, Zeist, the Netherlands.

Walinder MEP and Gardner DJ (1999) Factors influencing contact angle measurements on wood particles by column wicking. *Journal of Adhesion Science and Technology* **13(12)**: 1363–1374.